INSTITUTE OF PHYSICS PUBLISHING INVERSE PROBLEMS

Inverse Problems **19** (2003) 703–724 PII: S0266-5611(03)57780-2

Identification of elastic inclusions and elastic moment tensors by boundary measurements

Hyeonbae Kang[1], **Eunjoo Kim**[1] **and June-Yub Lee**[2]

[1] School of Mathematical Sciences, Seoul National University, Seoul 151-747, Korea
[2] Department of Mathematics, Ewha Women's University, Seoul 120-750, Korea

E-mail: hkang@math.snu.ac.kr, kej@math.snu.ac.kr and jylee@math.ewha.ac.kr

Received 30 December 2002, in final form 7 April 2003
Published 24 April 2003
Online at stacks.iop.org/IP/19/703

Abstract

We consider the problem of identifying unknown inclusions inside an elastic body by means of traction–displacement relations measured on the boundary. Based on the asymptotic formula of Ammari *et al* (2003 *J. Elast.* at press), we propose an algorithm to reconstruct unknown inclusions. The algorithm of this paper detects the location and the elastic moment tensors (elastic Pólya–Szegö tensors) of the inclusion. Since the elastic moment tensors carry information on the size of the inclusion, we can represent the inclusion in two dimensions by a disc of the detected size with the detected centre. We also propose an algorithm to find an ellipse which represents the elastic moment tensors. For this purpose, we explicitly compute elastic moment tensors associated with ellipses. Several results of numerical experiments are presented. We emphasize that only shear stresses are used for the reconstruction of the inclusion: linear traction to detect elastic moment tensors and quadratic polynomials to detect the location.

1. Introduction

Suppose that an elastic medium occupies a bounded domain Ω in $\mathbb{R}^d$, $d = 2, 3$, with a connected Lipschitz boundary $\partial\Omega$. Let the constants (λ, μ) denote the background Lamé coefficients that are the elastic parameters in the absence of any inhomogeneities. Suppose that the elastic inhomogeneity D in Ω is given by

$$D = \epsilon B + z \tag{1.1}$$

where B is a bounded Lipschitz domain in $\mathbb{R}^d$. Here the small number ϵ represents the order of magnitude of D and z its location. We assume that D is located away from $\partial\Omega$, i.e. there exists $c_0 > 0$ such that

$$\inf_{x\in D} \operatorname{dist}(x, \partial\Omega) > c_0. \tag{1.2}$$

0266-5611/03/030703+22$30.00

Suppose that D has the pair of Lamé constants $(\tilde{\lambda}, \tilde{\mu})$ which is different from that of the background elastic body, (λ, μ). It is always assumed that

$$\mu > 0, \qquad d\lambda + 2\mu > 0, \qquad \tilde{\mu} > 0 \qquad \text{and} \qquad d\tilde{\lambda} + 2\tilde{\mu} > 0. \tag{1.3}$$

We also assume that

$$(\lambda - \tilde{\lambda})(\mu - \tilde{\mu}) \geqslant 0, \qquad ((\lambda - \tilde{\lambda})^2 + (\mu - \tilde{\mu})^2 \neq 0). \tag{1.4}$$

We consider the problem of reconstructing the inclusion D by means of the traction–displacement relation measured on $\partial\Omega$. Throughout this paper the background Lamé constants λ, μ are assumed to be known. The purpose of this work is to reconstruct the unknown D with or without knowledge of $\tilde{\lambda}$, $\tilde{\mu}$.

The linear system of elastostatics with the traction boundary condition in the presence of an inclusion D takes the form

$$\begin{aligned} &\sum_{j,k,l=1}^{d} \frac{\partial}{\partial x_j}\left(C_{ijkl}\frac{\partial u_k}{\partial x_l}\right) = 0 \qquad \text{in } \Omega, i = 1, \ldots, d, \\ &\frac{\partial \vec{u}}{\partial \nu}\bigg|_{\partial\Omega} = \vec{g}, \end{aligned} \tag{1.5}$$

where $\vec{g}$ satisfies the usual compatibility condition, see [3], and $\frac{\partial}{\partial \nu}$ denotes the conormal derivative associated with the system of elastostatics, namely

$$\frac{\partial \vec{u}}{\partial \nu} := \lambda(\operatorname{div} \vec{u})N + \mu(\nabla \vec{u} + \nabla \vec{u}^{\mathrm{T}})N \qquad \text{on } \partial D, \tag{1.6}$$

where N is the outward unit normal to ∂D and T denotes the transpose. Here the piecewise constant Lamé parameter C_{ijkl} is given by

$$C_{ijkl} := (\lambda\chi(\Omega\backslash D) + \tilde{\lambda}\chi(D))\delta_{ij}\delta_{kl} + (\mu\chi(\Omega\backslash D) + \tilde{\mu}\chi(D))(\delta_{ik}\delta_{jl} + \delta_{il}\delta_{jk}), \tag{1.7}$$

where $\chi(D)$ is the characteristic function of D.

In [3], a complete asymptotic expansion of the solution u to (1.5) as $\epsilon \to 0$ was obtained. The first-order term was obtained in [1]. This asymptotic formula is given in terms of the background solution and generalized elastic moment tensors. The background solution is the solution to (1.5) when there is no inclusion, i.e. $D = \emptyset$. The notion of (generalized) elastic moment tensors (EMTs) is introduced in [3] and their important properties such as symmetry and positive-definiteness were proved. This notion generalizes the elastic Pólya–Szegö tensors associated with cavity or rigid inclusions [8–11]. Based on the asymptotic formula, an algorithm to detect the unknown inclusion is proposed in [3]. The algorithm detects the first-order EMTs and the location z. The size of the inclusion can then be estimated from the detected EMTs. We call this algorithm the *disc reconstruction algorithm*. We note that the algorithm of [3] uses only linear stresses. In this paper we propose a different method to detect the centre which uses quadratic polynomials. We compare these two methods by numerical examples. It turns out that the method using quadratic polynomials performs better in the presence of noise. We emphasize that the centre and size of the inclusion are estimated without knowledge of Lamé constants $\tilde{\lambda}$, $\tilde{\mu}$ of the inclusion.

We then propose another algorithm to reconstruct the inclusion in two dimensions. The procedure to estimate EMTs is the same as that in the disc reconstruction algorithm. Instead of directly estimating the size of D from the computed EMTs, we find an ellipse which can represent them. We call this algorithm the *ellipse reconstruction algorithm*. Observe that the mere size and centre do not represent a long and thin inclusion well. Thus we look for a geometric figure associated with the detected EMTs and the class of ellipses seems the most

natural class of geometric figures to be considered. For the purpose of finding the representing ellipse, we compute the first-order EMTs associated with ellipses. Note that the first-order EMTs associated with elliptic holes with $\tilde{\lambda} = \tilde{\mu} = 0$ are computed in [10] (see also [8]). We implement both algorithms and compare the performance of those two algorithms. It turns out that the ellipse reconstruction algorithm performs far better in estimating the size and orientation of the inclusion. But unlike the disc reconstruction algorithm, the ellipse reconstruction algorithm requires *a priori* knowledge of the Lamé constants $\tilde{\lambda}$, $\tilde{\mu}$ of the inclusion.

The algorithms proposed in this paper work for both two and three dimensions except for the representation of three-dimensional EMTs by geometric figures. For instance, the EMTs associated with ellipsoids have not been computed. It would be interesting to find a canonical representation of EMTs by certain geometric figures.

We have implemented the disc reconstruction algorithm and the ellipse reconstruction algorithm in 2D using Matlab. Examples for computational simulations were generated by a direct second-order finite-difference elasticity solver. The algorithms provide stable numerical results even with random noise on the boundary measurement. More precisely, the perturbations of constructed radius and centre position are linearly proportional to the noise level. The recovered centres are quite accurate but the computed radius does not exactly match with the original value when the disc reconstruction algorithm is used. We numerically investigate the proportional constant between computed and actual radius and find that it depends only on μ of the inclusion. The disc reconstruction method also gives pretty good approximated discs for general domains. The ellipse recovery method gives perfect results for discs and ellipses and good approximations for general domains.

This paper is organized as follows. In section 2, we review the notion of EMTs introduced in [3] and obtain their relation under rotation. In section 3 we review the asymptotic formula and the algorithm to detect the EMTs and centre by boundary measurements, and then propose a slightly different method to detect the centre. Section 4 presents the numerical results of the disc reconstruction algorithm. In section 5, EMTs associated with ellipses in 2D are computed and the ellipse reconstruction algorithm is proposed. Its numerical results are presented in section 6.

We want to add a brief comment on cases with multiple inclusions before concluding this section. The asymptotic formula in this paper and [3] is valid for multiple inclusions and may be used for detection of multiple inclusions. Based on the asymptotic expansion, one may use highly oscillating background solutions to develop Dirac mass at the location of inclusions. This method was used by Ammari *et al* [4] for detection of conductivity inhomogeneities. See the forthcoming paper [2] for this. Another method of detecting multiple conductivity inclusions was developed by Brühl *et al* [6] which uses finite spectral decomposition of the approximate Dirichlet-to-Neumann map. This approximation uses an asymptotic expansion. We emphasize that algorithms in this paper use at most $(2d - 1)$ linear or quadratic shear tractions.

2. Elastic moment tensor: rotation relation

The elastostatic system corresponding to the Lamé constants λ, μ is defined by

$$\mathcal{L}_{\lambda,\mu}\,\vec{u} := \mu\Delta\,\vec{u} + (\lambda+\mu)\nabla\mathrm{div}\,\vec{u}. \tag{2.1}$$

The Kelvin matrix of fundamental solutions $\Gamma = (\Gamma_{ij})$ for the Lamé system $\mathcal{L}_{\lambda,\mu}$ is defined as

$$\Gamma_{ij}(x) := \begin{cases} \dfrac{A}{4\pi}\dfrac{\delta_{ij}}{|x|} + \dfrac{B}{4\pi}\dfrac{x_i x_j}{|x|^3}, & \text{if } d = 3, \\ -\dfrac{A}{2\pi}\delta_{ij}\log|x| + \dfrac{B}{2\pi}\dfrac{x_i x_j}{|x|^2}, & x \neq 0, \text{ if } d = 2, \end{cases} \qquad i, j = 1, \ldots, d, \tag{2.2}$$

where

$$A = \frac{1}{2}\left(\frac{1}{\mu} + \frac{1}{2\mu+\lambda}\right) \qquad \text{and} \qquad B = \frac{1}{2}\left(\frac{1}{\mu} - \frac{1}{2\mu+\lambda}\right). \tag{2.3}$$

If we define $N\vec{f}$ for $\vec{f} \in C_0^\infty(\mathbb{R}^d)$ by

$$N\vec{f}(x) := \int_{\mathbb{R}^d} \Gamma(x-y)\vec{f}(y)\,\mathrm{d}y, \tag{2.4}$$

then $\mathcal{L}_{\lambda,\mu}(N\vec{f}) = \vec{f}$. The single- and double-layer potentials of the density function $\vec{\phi}$ on D associated with the Lamé parameters (λ, μ) are defined by

$$\mathcal{S}_D\vec{\phi}(x) := \int_{\partial D} \Gamma(x-y)\vec{\phi}(y)\,\mathrm{d}\sigma(y), \qquad x \in \mathbb{R}^d, \tag{2.5}$$

$$\mathcal{D}_D\vec{\phi}(x) := \int_{\partial D} \frac{\partial}{\partial \nu_y}\Gamma(x-y)\vec{\phi}(y)\,\mathrm{d}\sigma(y), \qquad x \in \mathbb{R}^d\backslash\partial D, \tag{2.6}$$

where $\frac{\partial}{\partial \nu}$ denotes the conormal derivative defined in (1.6).

As one can easily see, the fundamental solution Γ is not rotation invariant. In this section we find a rotation formula for Γ in two dimensions. Let R_θ be the rotation by θ, namely

$$R_\theta = \begin{pmatrix} \cos\theta & -\sin\theta \\ \sin\theta & \cos\theta \end{pmatrix}.$$

Lemma 2.1.

(i) $\mathcal{L}_{\lambda,\mu}(R_\theta^{-1}(\vec{u} \circ R_\theta)) = R_\theta^{-1}(\mathcal{L}_{\lambda,\mu}\vec{u}) \circ R_\theta$,
(ii) $\left(\frac{\partial \vec{u}}{\partial \nu}\right) \circ R_\theta = R_\theta \frac{\partial}{\partial \nu}(R_\theta^{-1}(\vec{u} \circ R_\theta))$.

Proof. One can derive formulae (i) and (ii) from the following formula which can be proved by elementary calculations:

$$(\operatorname{div}\vec{u}) \circ R_\theta = \operatorname{div}(R_\theta^{-1}(\vec{u} \circ R_\theta)),$$
$$R_\theta^{-1}(\nabla f) \circ R_\theta = \nabla(f \circ R_\theta).$$

This completes the proof. □

Lemma 2.2 (Rotation formula).

$$\Gamma(R_\theta(X)) = R_\theta\Gamma(X)R_\theta^{-1}, \qquad X \in \mathbb{R}^2. \tag{2.7}$$

Proof. For $\vec{f} \in C_0^\infty(\mathbb{R}^d)$, let $N\vec{f}$ be as defined in (2.4). Then

$$\begin{aligned} R_\theta^{-1}(N\vec{f})(R_\theta(x)) &= \int_{\mathbb{R}^d} R_\theta^{-1}\Gamma(R_\theta(x)-y)\vec{f}(y)\,\mathrm{d}y \\ &= \int_{\mathbb{R}^d} R_\theta^{-1}\Gamma(R_\theta(x-y))R_\theta R_\theta^{-1}\vec{f}(R_\theta(y))\,\mathrm{d}y. \end{aligned}$$

On the other hand, it follows from lemma 2.1(i) that

$$\mathcal{L}_{\lambda,\mu}(R_\theta^{-1}(N\vec{f})(R_\theta(x))) = R_\theta^{-1}(\mathcal{L}_{\lambda,\mu}N\vec{f})(R_\theta(x)) = R_\theta^{-1}\vec{f}(R_\theta(y)).$$

Thus we have

$$R_\theta^{-1}\Gamma(R_\theta(x-y))R_\theta = \Gamma(x-y),$$

and the proof is complete. □

As a consequence of (2.7) we obtain the following rotation formula for the single-layer potential.

Lemma 2.3. *Let $\hat{D}$ be a bounded domain in $\mathbb{R}^2$ and $D = R_\theta(\hat{D})$. Then for any vector potential $\vec{\varphi}$, we have*

$$(\mathcal{S}_D\vec{\varphi})(R_\theta(x)) = R_\theta \mathcal{S}_{\hat{D}}(R_\theta^{-1}(\vec{\varphi}\circ R_\theta))(x), \tag{2.8}$$

$$\frac{\partial}{\partial \nu}(\mathcal{S}_D\vec{\varphi})(R_\theta(x)) = R_\theta \frac{\partial}{\partial \nu}\mathcal{S}_{\hat{D}}(R_\theta^{-1}(\vec{\varphi}\circ R_\theta))(x). \tag{2.9}$$

Proof. Equation (2.8) immediately follows from (2.7). By lemma 2.1(ii), we get

$$\frac{\partial}{\partial \nu}(\mathcal{S}_D\vec{\varphi})(R_\theta(x)) = R_\theta \frac{\partial}{\partial \nu}(R_\theta^{-1}(\mathcal{S}_D\vec{\varphi})\circ R_\theta)(x).$$

Then (2.9) follows from (2.8) and the above identity. This completes the proof. □

We now review the results of [3] on the properties of EMTs and then establish their relations under rotation. In [3] the notion of EMTs associated with Lamé parameters λ, μ, $\tilde{\lambda}$, $\tilde{\mu}$ and a domain B were defined as follows. For multi-index $\alpha \in \mathbb{N}^d$ and $j = 1, \ldots, d$ let $\vec{f}_\alpha^{\,j}$ and $\vec{g}_\alpha^{\,j}$ in $L^2(\partial B)$ be the solution of

$$\begin{aligned} &\tilde{\mathcal{S}}_B \vec{f}_\alpha^{\,j}|_+ - \mathcal{S}_B \vec{g}_\alpha^{\,j}|_- = x^\alpha e_j|_{\partial B}, \\ &\frac{\partial}{\partial \tilde{\nu}}\tilde{\mathcal{S}}_B \vec{f}_\alpha^{\,j}\bigg|_+ - \frac{\partial}{\partial \nu}\mathcal{S}_B \vec{g}_\alpha^{\,j}\bigg|_- = \frac{\partial (x^\alpha e_j)}{\partial \nu}\bigg|_{\partial B}. \end{aligned} \tag{2.10}$$

Here $u|_+$ and $u|_-$ denote the limits from inside and outside D, respectively, and e_j denotes a unit vector in the x^j-direction. For $\beta \in \mathbb{N}^d$, the *elastic moment tensor* $M_{\alpha\beta}^j$ associated with the domain B and Lamé parameters (λ, μ) for the background and $(\tilde{\lambda}, \tilde{\mu})$ for B is defined by

$$M_{\alpha\beta}^j = (m_{\alpha\beta 1}^j, m_{\alpha\beta 2}^j, m_{\alpha\beta 3}^j) = \int_{\partial B} y^\beta \vec{g}_\alpha^{\,j}(y)\, d\sigma(y). \tag{2.11}$$

When $|\alpha| = |\beta| = 1$, we make a slight change of notation: when $\alpha = e_i$ and $\beta = e_p$, $i, p = 1, \ldots, d$, put $m_{pq}^{ij} := m_{\alpha\beta q}^j$, $q, j = 1, \ldots, d$. So, if we put $\vec{g}_i^{\,j} := \vec{g}_\alpha^{\,j}$, then

$$m_{pq}^{ij} = \int_{\partial B} y_p e_q \cdot \vec{g}_i^{\,j}\, d\sigma(y). \tag{2.12}$$

The following two theorems are proved in [3].

Theorem 2.4 (Symmetry). *For $p, q, i, j = 1, \ldots, d$, the following holds:*

$$m_{pq}^{ij} = m_{qp}^{ij}, \qquad m_{pq}^{ij} = m_{pq}^{ji}, \qquad \text{and} \qquad m_{pq}^{ij} = m_{ij}^{pq}. \tag{2.13}$$

Theorem 2.5 (Positive-definiteness). *Let $M = (m_{pq}^{ij})$. If $\mu > \tilde{\mu}$ ($\mu < \tilde{\mu}$, respectively), then M is positive (negative, respectively) definite on the space of symmetric matrices. Let κ be an eigenvalue of M. Then there are constants C_1 and C_2 depending only on $\lambda, \mu, \tilde{\lambda}, \tilde{\mu}$ and the Lipschitz character of B such that*

$$C_1|B| \leqslant |\kappa| \leqslant C_2|B|. \tag{2.14}$$

Theorems 2.4 and 2.5 imply that M becomes an anisotropic elastic tensor.

Note that $\vec{u}$ defined by

$$\vec{u}(x) := \begin{cases} \tilde{\mathcal{S}}\vec{f}_i^{\,j}(x), & x \in D, \\ \mathcal{S}\vec{g}_i^{\,j}(x) + x_i e_j, & x \in \mathbb{R}^d \backslash \bar{D} \end{cases}$$

is the unique solution of the transmission problem

$$\begin{aligned}
&\mathcal{L}_{\lambda,\mu}\,\vec{u} = 0 && \text{in } \mathbb{R}^d\backslash\bar{D},\\
&\mathcal{L}_{\tilde{\lambda},\tilde{\mu}}\,\vec{u} = 0 && \text{in } D,\\
&\vec{u}|_+ - \vec{u}|_- = 0 && \text{on } \partial D,\\
&\left.\frac{\partial\,\vec{u}}{\partial\tilde{\nu}}\right|_+ - \left.\frac{\partial\,\vec{u}}{\partial\nu}\right|_- = 0 && \text{on } \partial D,\\
&\vec{u}(x) - x_i e_j = \mathrm{O}(|x|^{1-d}), && \text{as } |x|\to\infty.
\end{aligned} \tag{2.15}$$

It was shown in [3], (5.14) that

$$m^{ij}_{pq} = \int_{\partial D}\left[\frac{\partial(x_p e_q)}{\partial\nu} - \frac{\partial(x_p e_q)}{\partial\tilde{\nu}}\right]\cdot\,\vec{u}|_+\,\mathrm{d}\sigma. \tag{2.16}$$

Lemma 2.6. *Let $\hat{D}$ be a bounded Lipschitz domain in $\mathbb{R}^2$ and $D = R_\theta(\hat{D})$. Let*

$$R_\theta = \begin{pmatrix}\cos\theta & -\sin\theta\\ \sin\theta & \cos\theta\end{pmatrix} := \begin{pmatrix} r_{11} & r_{12}\\ r_{21} & r_{22}\end{pmatrix}.$$

Let m^{ij}_{pq} and $\hat{m}^{ij}_{pq}$, $i, j, p, q = 1, 2$, denote EMTs associated with D and $\hat{D}$, respectively. Then,

$$m^{ij}_{pq} = \sum_{u,v=1}^{2}\sum_{k,l=1}^{2}(-1)^{j+l+q+v} r_{pu} r_{vq} r_{ik} r_{lj}\hat{m}^{kl}_{uv}. \tag{2.17}$$

Proof. For $i, j = 1, 2$, let $\vec{f}^{\,j}_i$ and $\vec{g}^{\,j}_i$ be the solution of

$$\begin{aligned}
&\tilde{\mathcal{S}}_D\vec{f}^{\,j}_i|_+ - \mathcal{S}_D\vec{g}^{\,j}_i|_- = x_i e_j|_{\partial D},\\
&\left.\frac{\partial}{\partial\tilde{\nu}}\tilde{\mathcal{S}}_D\vec{f}^{\,j}_i\right|_+ - \left.\frac{\partial}{\partial\nu}\mathcal{S}_D\vec{g}^{\,j}_i\right|_- = \left.\frac{\partial(x_i e_j)}{\partial\nu}\right|_{\partial D},
\end{aligned} \tag{2.18}$$

and let $\hat{f}^{\,j}_i$ and $\hat{g}^{\,j}_i$ be the solution of (2.18) with D replaced with $\hat{D}$. It then follows from lemmas 2.1(ii) and 2.3 that

$$\tilde{\mathcal{S}}_{\hat{D}}(R_\theta^{-1}(\vec{f}^{\,j}_i\circ R_\theta))|_+ - \mathcal{S}_{\hat{D}}(R_\theta^{-1}(\vec{g}^{\,j}_i\circ R_\theta))|_- = R_\theta^{-1}((x_i e_j)\circ R_\theta)|_{\partial\hat{D}},$$

$$\left.\frac{\partial}{\partial\tilde{\nu}}\tilde{\mathcal{S}}_{\hat{D}}(R_\theta^{-1}(\vec{f}^{\,j}_i\circ R_\theta))\right|_+ - \left.\frac{\partial}{\partial\nu}\mathcal{S}_{\hat{D}}(R_\theta^{-1}(\vec{g}^{\,j}_i\circ R_\theta))\right|_- = \left.\frac{\partial}{\partial\nu}(R_\theta^{-1}((x_i e_j)\circ R_\theta))\right|_{\partial\hat{D}}.$$

It is easy to see that

$$R_\theta^{-1}((x_i e_j)\circ R_\theta) = R_\theta(x)_i R_\theta^{-1}(e_j) = \sum_{k,l=1}^{2}(-1)^{j+l} r_{ik} r_{lj}(x_k e_l), \qquad i, j = 1, 2.$$

It then follows from the uniqueness of the solution to the integral equation (2.10) that

$$R_\theta^{-1}(\vec{g}^{\,j}_i\circ R_\theta) = \sum_{k,l=1}^{2}(-1)^{j+l} r_{ik} r_{lj}\hat{g}^l_k, \qquad i, j = 1, 2.$$

By (2.12) and a change of variables, we have

$$\begin{aligned}
m^{ij}_{pq} &= \int_{\partial D} x_p e_q\cdot\vec{g}^{\,j}_i\,\mathrm{d}\sigma\\
&= \int_{\partial\hat{D}} R_\theta^{-1}((x_p e_q)\circ R_\theta)\cdot R_\theta^{-1}(\vec{g}^{\,j}_i\circ R_\theta)\,\mathrm{d}\sigma\\
&= \sum_{u,v=1}^{2}\sum_{k,l=1}^{2}(-1)^{j+l+q+v} r_{pu} r_{vq} r_{ik} r_{lj}\hat{m}^{kl}_{uv}.
\end{aligned}$$

The proof is complete. □

3. Asymptotic formulae and detection algorithms

For a given traction boundary $\vec{g}$, let $\vec{u}$ be the solution of the problem (1.5). Define the function $\vec{H}[\vec{g}]$ by

$$\vec{H}[\vec{g}](x) = -\mathcal{S}_\Omega(\vec{g})(x) + \mathcal{D}_\Omega(\vec{f})(x), \qquad x \in \mathbb{R}^d \backslash \partial\Omega,\ \vec{f} := \vec{u}|_{\partial\Omega}, \tag{3.1}$$

where $\mathcal{S}_\Omega$ and $\mathcal{D}_\Omega$ are the single- and double-layer potentials for the Lamé system on $\partial\Omega$. The following asymptotic formula for $\vec{H}[\vec{g}]$ is obtained in [3].

Theorem 3.1. *For $x \in \mathbb{R}^d \backslash \bar{\Omega}$,*

$$\vec{H}[\vec{g}](x) = \sum_{j=1}^{d} \sum_{|\alpha|=1}^{d} \sum_{|\beta|=1}^{d+1-|\alpha|} \frac{\epsilon^{|\alpha|+|\beta|+d-2}}{\alpha!\beta!} (\partial^\alpha U_j)(z) \partial^\beta \Gamma(x-z) M^j_{\alpha\beta} + \mathrm{O}\left(\frac{\epsilon^{2d}}{|x|^{d-1}}\right), \tag{3.2}$$

where $\vec{U}$ is a solution of homogeneous elastostatic equation (1.5), $M^j_{\alpha\beta}$ are the EMTs defined by (2.11), and Γ is the Kelvin matrix of fundamental solutions corresponding to the Lamé parameters (λ, μ).

If $\vec{U}$ is linear, then $\partial^\alpha \vec{U} = 0$ if $|\alpha| > 1$ and hence

$$\vec{H}[\vec{g}](x) = \epsilon^d \sum_{j=1}^{d} \sum_{|\alpha|=1} \sum_{|\beta|=1} (\partial^\alpha U_j)(z) \partial^\beta \Gamma(x-z) M^j_{\alpha\beta} + \mathrm{O}\left(\frac{\epsilon^d}{|x|^d}\right) + \mathrm{O}\left(\frac{\epsilon^{2d}}{|x|^{d-1}}\right), \tag{3.3}$$

or, for $k = 1, \ldots, d$,

$$H_k[\vec{g}](x) = \epsilon^d \sum_{i,j,p,q=1}^{d} (\partial_i U_j)(z) \partial_p \Gamma_{kq}(x-z) m^{ij}_{pq} + \mathrm{O}\left(\frac{\epsilon^d}{|x|^d}\right) + \mathrm{O}\left(\frac{\epsilon^{2d}}{|x|^{d-1}}\right). \tag{3.4}$$

For a general g, we have the following formula:

$$H_k[\vec{g}](x) = \epsilon^d \sum_{i,j,p,q=1}^{d} (\partial_i U_j)(z) \partial_p \Gamma_{kq}(x-z) m^{ij}_{pq} + \mathrm{O}\left(\frac{\epsilon^d}{|x|^d}\right) + \mathrm{O}\left(\frac{\epsilon^{d+1}}{|x|^{d-1}}\right). \tag{3.5}$$

Since $\partial_p \Gamma_{kq}(x-z) = \partial_p \Gamma_{kq}(x) + \mathrm{O}(|x|^d)$, (3.4) and (3.5) yield the following far-field relations.

Theorem 3.2. *If $|x| = \mathrm{O}(\epsilon^{-1})$, then*

$$|x|^{d-1} H_k[\vec{g}](x) = \epsilon^d |x|^{d-1} \sum_{i,j,p,q=1}^{d} (\partial_i U_j)(z) \partial_p \Gamma_{kq}(x) m^{ij}_{pq}, \qquad \textit{modulo } \mathrm{O}(\epsilon^{d+1}). \tag{3.6}$$

Moreover, if $\vec{U}$ is linear, then for all x with $|x| = \mathrm{O}(\epsilon^{-d})$, then

$$|x|^{d-1} H_k[\vec{g}](x) = \epsilon^d |x|^{d-1} \sum_{i,j,p,q=1}^{d} (\partial_i U_j)(z) \partial_p \Gamma_{kq}(x) m^{ij}_{pq}, \qquad \textit{modulo } f\mathrm{O}(\epsilon^{2d}). \tag{3.7}$$

We now explain the method proposed in [3] to reconstruct the scaled EMT $\epsilon^d m^{ij}_{pq}$, $i, j, p, q = 1, \ldots, d$, and the location z of the elastic inclusion D. This method is based on (3.4) and (3.7). In addition to this method, we propose a new method to detect the location based on (3.6).

3.1. Determination of EMT

Easy computations show that

$$\partial^p \Gamma_{kq}(x) = -\frac{A}{\omega_d}\frac{\delta_{kq}x_p}{|x|^d} + \frac{B}{\omega_d}\frac{\delta_{kp}x_q + \delta_{pq}x_k}{|x|^d} - \frac{dB}{\omega_d}\frac{x_k x_q x_p}{|x|^{d+2}}, \tag{3.8}$$

where $\omega_d = 2\pi$ if $d = 2$ and $\omega_d = 4\pi$ if $d = 3$. If $x = te_l$, $t \in \mathbb{R}$, $l = 1, \ldots, d$, then

$$\begin{aligned}\partial^p \Gamma_{kq}(te_l) &= \frac{1}{\omega_d t^{d-1}}[-A\delta_{kq}\delta_{pl} + B(\delta_{kp}\delta_{ql} + \delta_{kl}\delta_{pq}) - dB\delta_{kl}\delta_{ql}\delta_{pl}] \\ &:= \frac{1}{\omega_d t^{d-1}} e_{klpq}. \end{aligned} \tag{3.9}$$

For $u, v = 1, \ldots, d$, let

$$\vec{g}_{uv} := \left.\frac{\partial(x_u e_v + x_v e_u)}{\partial \nu}\right|_{\partial\Omega}. \tag{3.10}$$

Then the corresponding background solution $\vec{U}$ is given by $\vec{U}(x) = x_u e_v + x_v e_u$. Thus $\partial_i U_j(z) = \delta_{iu}\delta_{jv} + \delta_{iv}\delta_{ju}$ and hence the right-hand side of (3.7) equals

$$\frac{\epsilon^d}{\omega_d}\sum_{i,j,p,q=1}^{d}(\delta_{iu}\delta_{jv} + \delta_{iv}\delta_{ju})e_{klpq}m^{ij}_{pq} = 2\frac{\epsilon^d}{\omega_d}\sum_{p,q=1}^{3} e_{klpq}m^{uv}_{pq}.$$

The last equality is valid since $m^{uv}_{pq} = m^{vu}_{pq}$. It then follows from (3.4) that if $t = \mathrm{O}(\epsilon^{-d})$, then, modulo $\mathrm{O}(\epsilon^{2d})$,

$$t^{d-1}H_k[\vec{g}_{uv}](te_l) = \begin{cases} \dfrac{2\epsilon^d}{\omega_d}\left[-(A + (d-2)B)m^{uv}_{kk} + B\displaystyle\sum_{i\neq k} m^{vu}_{ii}\right], & \text{if } k = l, \\ \dfrac{2\epsilon^d}{\omega_d}(B - A)m^{uv}_{kl}, & \text{if } k \neq l. \end{cases} \tag{3.11}$$

Let

$$h^{uv}_{kl} := \lim_{t\to\infty} t^{d-1}H_k[\vec{g}_{uv}](te_l), \qquad k, l, u, v = 1, \ldots, d. \tag{3.12}$$

Then the entries m^{uv}_{kl}, $u, v, k, l = 1, \ldots, d$, of the EMT can be recovered, modulo $\mathrm{O}(\epsilon^{2d})$, as follows: for $u, v, k, l = 1, \ldots, d$,

$$\epsilon^d m^{uv}_{kl} = \begin{cases} -\dfrac{\omega_d\mu(\lambda + (d-1)\mu)}{d\lambda + (d^2 - 2d + 2)\mu}\left[\dfrac{\lambda + (d-2)\mu}{2\mu}\displaystyle\sum_{j=1}^{d} h^{uv}_{jj} + h^{uv}_{kk}\right], & k = l, \\ -\dfrac{\omega_d}{2}(\lambda + (d-1)\mu)h^{uv}_{kl}, & k \neq l. \end{cases} \tag{3.13}$$

3.2. Determination of size

By corollary 5.5 of [3], if $i \neq j$, then

$$\mu\left|\frac{\mu - \tilde{\mu}}{\mu + \tilde{\mu}}\right||D| \leqslant |\epsilon^d m^{ij}_{ij}| \leqslant C|D|. \tag{3.14}$$

Thus we take as an estimation of size

$$\left|\frac{\mu + \tilde{\mu}}{\mu(\mu - \tilde{\mu})}\right||\epsilon^d m^{ij}_{ij}| \tag{3.15}$$

if $\tilde{\mu}$ is known, otherwise $\frac{\mu+\tilde{\mu}}{\mu(\mu-\tilde{\mu})}$ is assumed to be 1.

3.3. Determination of the location: linear method

Having found $\epsilon^d m_{kp}^{uv}$, we now proceed to find the centre z. In view of (3.4), we have

$$2\epsilon^d \sum_{p,q=1}^{d} \partial^p \Gamma_{kq}(x-z) m_{pq}^{uv} = H_k[\vec{g}_{uv}](x) + \mathrm{O}\left(\frac{\epsilon^d}{|x|^d}\right) + \mathrm{O}\left(\frac{\epsilon^{2d}}{|x|^{d-1}}\right), \quad k, u, v = 1, \ldots, d. \tag{3.16}$$

Since $m_{pq}^{uv} = m_{qp}^{vu}$, we can symmetrize (3.16) to obtain

$$\epsilon^d \sum_{p,q=1}^{d} [\partial^p \Gamma_{kq}(x-z) + \partial^q \Gamma_{kp}(x-z)] m_{pq}^{uv} = H_k[\vec{g}_{uv}](x) + \mathrm{O}\left(\frac{\epsilon^d}{|x|^d}\right) + \mathrm{O}\left(\frac{\epsilon^{2d}}{|x|^{d-1}}\right). \tag{3.17}$$

Define the transform P on the space V of $d \times d$ symmetric matrices by

$$P((a_{pq})) = \left(\sum_{p,q=1} a_{pq} \epsilon^d m_{pq}^{uv}\right).$$

Then, by theorem 2.5, P is invertible on V. Let (n_{pq}^{ij}) be the matrix for P^{-1} on V, namely

$$P^{-1}((a_{pq})) = \left(\sum_{p,q=1} a_{pq} n_{pq}^{ij}\right), \qquad (a_{pq}) \in V. \tag{3.18}$$

It then follows from (3.17) that

$$\partial^p \Gamma_{kq}(x-z) + \partial^q \Gamma_{kp}(x-z) = \sum_{i,j=1}^{d} H_k[\vec{g}_{ij}](x) n_{ij}^{pq} + \mathrm{O}\left(\frac{1}{|x|^d}\right) + \mathrm{O}\left(\frac{\epsilon^d}{|x|^{d-1}}\right). \tag{3.19}$$

Observe from (3.8) that

$$\sum_{p=1}^{d} \partial^p \Gamma_{kp}(x-z) = \frac{B-A}{\omega_d} \frac{x_k - z_k}{|x-z|^d} = \frac{-1}{\omega_d((d-1)\mu+\lambda)} \frac{x_k - z_k}{|x-z|^d}, \qquad k = 1, \ldots, d.$$

Hence we obtain from (3.19) that

$$\frac{x_k - z_k}{|x-z|^d} = -\omega_d((d-1)\mu+\lambda) \sum_{i,j=1}^{d} H_k[\vec{g}_{ij}](x) \sum_{p=1}^{d} n_{ij}^{pp} + \mathrm{O}\left(\frac{1}{|x|^d}\right) + \mathrm{O}\left(\frac{\epsilon^d}{|x|^{d-1}}\right). \tag{3.20}$$

Multiplying both sides of (3.20) by $|x|^{d-1}$, we arrive at the following formula. If $|x| = \mathrm{O}(\epsilon^{-d})$, then

$$\frac{x_k - z_k}{|x-z|} = -\omega_d((d-1)\mu+\lambda)|x|^{d-1} \sum_{i,j=1}^{d} H_k[\vec{g}_{ij}](x) \sum_{p=1}^{d} n_{ij}^{pp} + \mathrm{O}(\epsilon^d), \quad k = 1, \ldots, d. \tag{3.21}$$

Formula (3.21) says that we can recover $\frac{x_k - z_k}{|x-z|}$, $k = 1, \ldots, d$, from the moment matrix, or the boundary measurements. We now use an idea from [7] and [5] to recover the centre z from $\frac{x-z}{|x-z|}$. Fix k and freeze x_l, $l \neq k$, so that $\sum_{l \neq k} |x_l| = \mathrm{O}(\epsilon^{-d})$. Then consider $-\omega_d((d-1)\mu+\lambda)|x|^{d-1} \sum_{i,j=1}^{d} H_k[\vec{g}_{ij}](x) \sum_{p=1}^{d} n_{ij}^{pp}$ as a function of x_k. In fact, for $x = x_k e_k + \sum_{l \neq k} x_l e_l$, define

$$\Phi_k(x_k) = -\omega_d((d-1)\mu+\lambda)|x|^{d-1} \sum_{i,j=1}^{d} H_k[\vec{g}_{ji}](x) \sum_{p=1}^{d} n_{ij}^{pp}. \tag{3.22}$$

We then find the unique zero of Φ_k, say z_k^*. Then the point $(z_1^*, \ldots, z_d^*)$ is the centre z within the precision of $\mathrm{O}(\epsilon^d)$. Here e_j is the usual coordinate vector, i.e. $e_j = (\delta_{ij})_{i=1,\ldots,d}$.

3.4. Determination of the location: quadratic method

This method uses the relation (3.6). In view of (3.6) and (3.9), we get

$$t^{d-1} H_k[\vec{g}](te_l) = \frac{1}{\omega_d} \sum_{i,j,p,q=1}^{d} (\partial_i U_j)(z) e_{klpq} \epsilon^d m^{ij}_{pq}, \qquad \text{modulo } \mathrm{O}(\epsilon^{d+1}). \tag{3.23}$$

Since $m^{ij}_{pq} = m^{ij}_{qp}$, we get

$$\sum_{i,j,p,q=1}^{d} (\partial_i U_j)(z) e_{klpq} \epsilon^d m^{ij}_{pq} = \tfrac{1}{2} \sum_{p,q=1}^{d} (e_{klpq} + e_{klqp}) \sum_{i,j=1}^{d} (\partial_i U_j)(z) \epsilon^d m^{ij}_{pq}.$$

Define a linear transform $T : \mathbb{R}^{d\times d} \to \mathbb{R}^{d\times d}$ by

$$T(a_{pq}) := \tfrac{1}{2} \sum_{p,q=1}^{d} (e_{klpq} + e_{klqp}) a_{pq}.$$

Then one can easily check that T is invertible. It then follows from (3.23) that

$$\sum_{i,j=1}^{d} (\partial_i U_j)(z) \epsilon^d m^{ij}_{pq} = \omega_d T^{-1}(t^{d-1} H_k[\vec{g}](te_l))_{pq}, \qquad \text{modulo } \mathrm{O}(\epsilon^{d+1}). \tag{3.24}$$

We then apply second-order homogeneous solutions for $\vec{U}$. In fact, in the two-dimensional case, take

$$\vec{U}(x) = (2x_1x_2, x_1^2 - x_2^2), \tag{3.25}$$

and $\vec{g} = \frac{\partial \vec{U}}{\partial \nu}$. Then using (3.24), we can determine $(\partial_i U_j)(z)$ (thus z) from the elastic moment tensor m^{ij}_{pq} and the limit value of $H_k[\vec{g}]$ at $t \to \infty$. In the three-dimensional case, we apply two homogeneous polynomials:

$$\vec{U}(x) = (2x_1x_2, x_1^2 - x_2^2, 0), \qquad (2x_1x_3, 0, x_1^2 - x_3^2). \tag{3.26}$$

4. Numerical results

Our disc identification algorithms do not rely on a forward solver while many iterative algorithms require a sequence of forward solutions. Solutions of the elasticity problem obtained by a second-order finite-difference forward solver are used only for generation of numerical simulations. In example 1, we show the physical configuration of a test example and convergence of the forward solver. Effectiveness and stability of the algorithms for a disc inclusion are numerically demonstrated in example 2 and validity of the asymptotic expansions for the radius and the centres has been checked under various physical configurations in example 3. Example 4 shows that the disc reconstruction algorithm also provides pretty good disc approximations even for domains with non-circular inclusions.

Example 1 (Forward solver). In this example, we compute four inhomogeneous solutions of (1.5) on a domain with a circular inclusion. The disc centred at $(0.4, 0.2)$ is of radius $r = 0.2$ and has Lamé constants $(\tilde{\lambda}, \tilde{\mu}) = (9, 6)$ while the background Lamé constants are $(\lambda, \mu) = (6, 4)$. $u^{1,1}$, $u^{1,2}$, $u^{2,2}$ and u^{quad} denote the inhomogeneous solutions with the same boundary values of the corresponding homogeneous solutions, $U^{1,1} = (2x, 0)$, $U^{1,2} = (y, x)$, $U^{2,2} = (0, y)$, $U^{quad} = (2xy, x^2 - y^2)$, respectively. Figure 1 shows the physical configuration of the inclusion. The solid and the dotted contour curves represent the positive and negative difference between inhomogeneous and homogeneous solutions and separation between contour curves is 0.01.

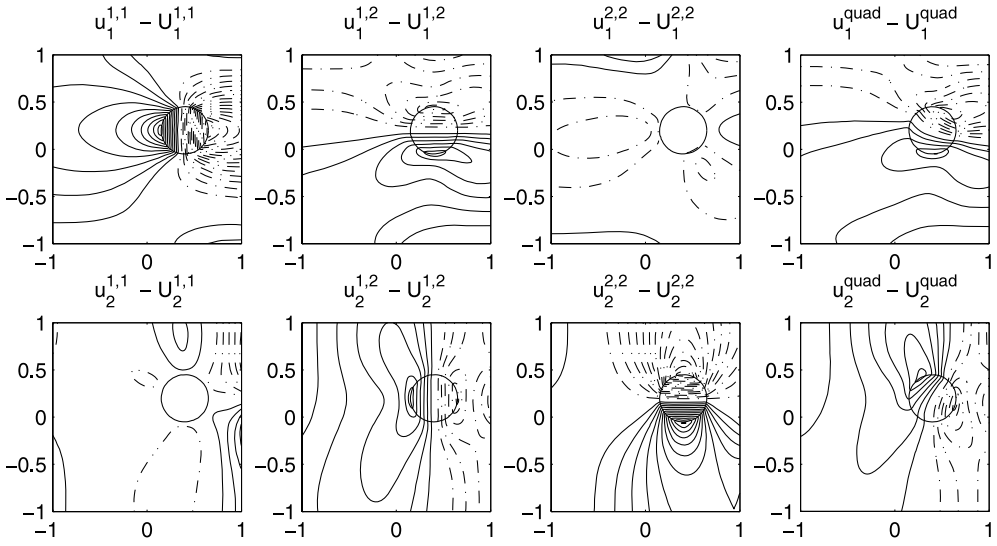

Figure 1. Difference between inhomogeneous and homogeneous solutions with $(\tilde{\lambda}, \tilde{\mu}) = (9, 6)$ and $(\lambda, \mu) = (6, 4)$.

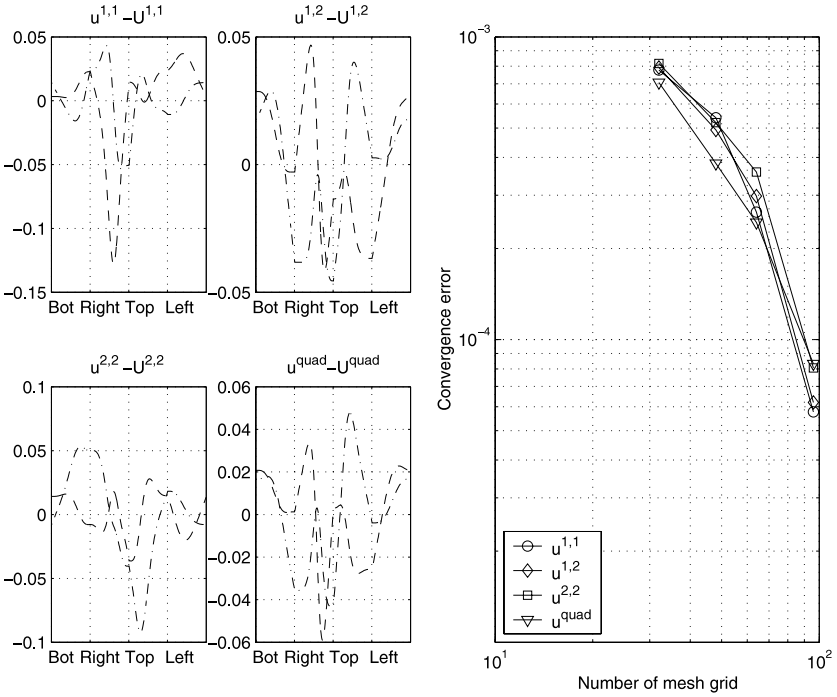

Figure 2. Difference between the inhomogeneous and the homogeneous solutions along four sides of the boundary and the convergence error of the forward solver for $N = 32$–96.

The four small plots in figure 2 show computed inhomogeneous solutions on a 128×128 grid compared to the homogeneous solutions. The dashed curve gives the first component perturbation $u_1|_{\partial\Omega} - U_1|_{\partial\Omega}$ along the four boundaries in a counterclockwise manner and the

dash–dotted line shows $u_2|_{\partial\Omega} - U_2|_{\partial\Omega}$. We compare the forward solutions on 32×32, 48×48, 64×64, and 96×96 coarse grids with those on the fine 128×128 grid in order to check the convergence and the accuracy of our numerical forward solver. The right-hand side plot in figure 2 draws the convergence error in root mean square norm as a function of discretization points and it shows that the solver has second-order numerical convergence and provides about four-digit accuracy with $N = 128$.

Example 2 (Computational results and stability of the algorithm). We have implemented the following reconstruction procedure for two-dimensional domains using Matlab and tested its performance using a circular inclusion as described in the previous example.

Step R. Compute $\epsilon^2 m_{kl}^{uv}$ using (3.12),

$$h_{kl}^{uv} := \lim_{t\to\infty} t H_k[\vec{g}_{uv}](te_l),$$

and m_{kl}^{uv} in (3.13) for $u \leqslant v$, $k \leqslant l$, $u \leqslant k$, and $v \leqslant l$:

$$\epsilon^2 m_{kl}^{uv} = \begin{cases} -\pi\mu\left[\dfrac{\lambda}{2\mu}\displaystyle\sum_{j=1}^{2} h_{jj}^{uv} + h_{kk}^{uv}\right], & k = l, \\ -\pi(\lambda+\mu)h_{kl}^{uv}, & k \neq l. \end{cases}$$

Then the computed radius r_c is $\sqrt{\frac{|m_{12}^{12}|}{\pi}}$.

Step C1. Compute the matrix $(n_{ij}^{pq})_{i,j,p,q=1,2}$ defined in (3.18):

$$\left(\sum_{p,q=1}^{2} a_{pq} n_{pq}^{ij}\right) := P^{-1}((a_{pq})) \qquad \text{where } P((a_{pq})) = \left(\sum_{p,q=1}^{2} a_{pq}\epsilon^2 m_{pq}^{uv}\right).$$

Then find the unique zero z_k^*, $k = 1, 2$, defined in (3.22),

$$\Phi_k(x_k) = -2\pi(\mu+\lambda)|x| \sum_{i,j=1}^{2} H_k[\vec{g}_{ji}](x) \sum_{p=1}^{2} n_{ij}^{pp}$$

by Newton's method with $H_k[\vec{g}_{ji}](x)$ and $\frac{\partial}{\partial x_k} H_k[\vec{g}_{ji}](x)$. In the iteration, the other coordinate x_{2-k} is frozen to a constant larger than $O(\epsilon^{-2})$ and we just choose x_{2-k} to be 10^3.

Step C2. Compute the centre point z using (3.24):

$$\sum_{i,j=1}^{2} (\partial_i U_j)(z)\epsilon^2 m_{pq}^{ij} = 2\pi T^{-1}(t H_k[\vec{g}](te_l))_{pq},$$

where

$$T(a_{pq}) := \tfrac{1}{2}\sum_{p,q=1}^{2} (e_{klpq} + e_{klqp})a_{pq}, \qquad \vec{U}(x) = (2x_1x_2, x_1^2 - x_2^2).$$

The following table summarizes a computational result of the algorithm using the forward solutions on a 128×128 mesh. r^c is the computed radius in step R, (x_1^c, y_1^c) is the centre obtained by the linear method in step C1, and (x_2^c, y_2^c) by the quadratic method in step C2.

(λ, μ)	$(\tilde{\lambda}, \tilde{\mu})$	(x, y)	r	r^c	(x_1^c, y_1^c)	(x_2^c, y_2^c)
(6, 4)	(9,6)	(0.4, 0.2)	0.25	0.3036	(0.4110, 0.1961)	(0.3983, 0.1985)

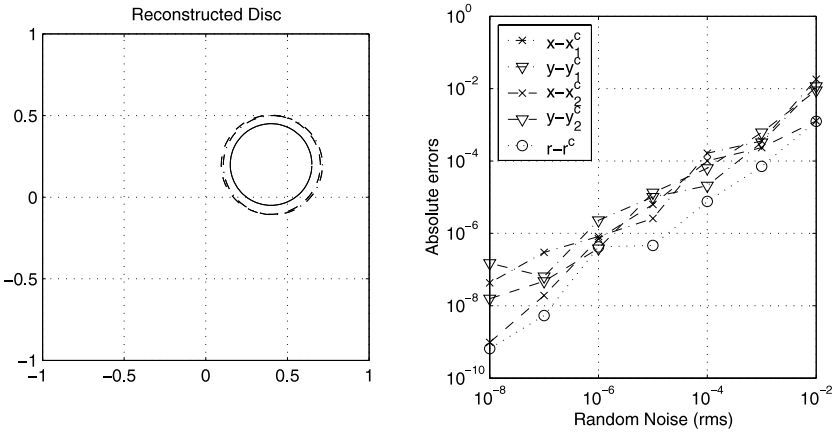

Figure 3. The dash–dotted circle represents the solution by the linear method and the dashed circle that by the quadratic method. The right-hand plot shows the perturbation error due to the random boundary noise.

The left-hand diagram in figure 3 shows the original disc as a solid curve; the dash–dotted circle is the reconstructed disc by the linear disc reconstruction method and the dashed circle is by the quadratic reconstruction method. In order to check the stability of the algorithm, we add random white noise to the Neumann and Dirichlet boundary data. Since computational results for radius and centres have some errors even without noise, we compare the difference between those with and without noise. We plot the absolute perturbation error of the reconstructed values with respect to white random noise level measured in the root mean square sense. The right-hand plot in figure 3 demonstrates that the algorithm is linearly stable with respect to the random boundary noise.

Example 3 (Asymptotic expansion). In this example, we test the computational algorithms described in the previous example with various configurations of disc inclusions and check the validity of the asymptotic expansions for the radius in case where the inclusion has finite size much bigger than 0. Table 1 and figure 4 summarize the computational results for three different locations with two different Lamé parameter configurations. The linear and the quadratic methods compute the centre quite well but the radii of the top three cases are about 20% larger than the original discs and those of the bottom cases are about 30% smaller than the originals.

In order to check the validity of the asymptotic expansion, we compute the radii by the disc reconstruction method for various combinations of radii and Lamé parameters while fixing the centre of inclusion at $(0.4, 0.2)$. We use three different computational grids to check the computational accuracy of our forward and inverse solvers. In figure 5, the dotted line is used for the results on 48×48, the dashed line on a 64×64, and the solid line on the 128×128 grid; the computational results on the three different grids seem to be almost identical. The figure also shows that the computed radius is not identical but proportional to the original value. The ratio between the computed and the original radius is independent of the radius, which is strong evidence of a missing second-order asymptotic expansion term for the radius. It is worth noting that the asymptotic expansion of EMT in (3.13) is correct up to $O(\epsilon^{2d})$, which gives a valid expression for the radius up to second-order accuracy in two dimensions.

Figure 6 illustrates the computed radius for a disc inclusion of radius $r = 0.25$ on a 64×64 grid with various Lamé constants. It shows that the computed radius is dependent only on μ_1,

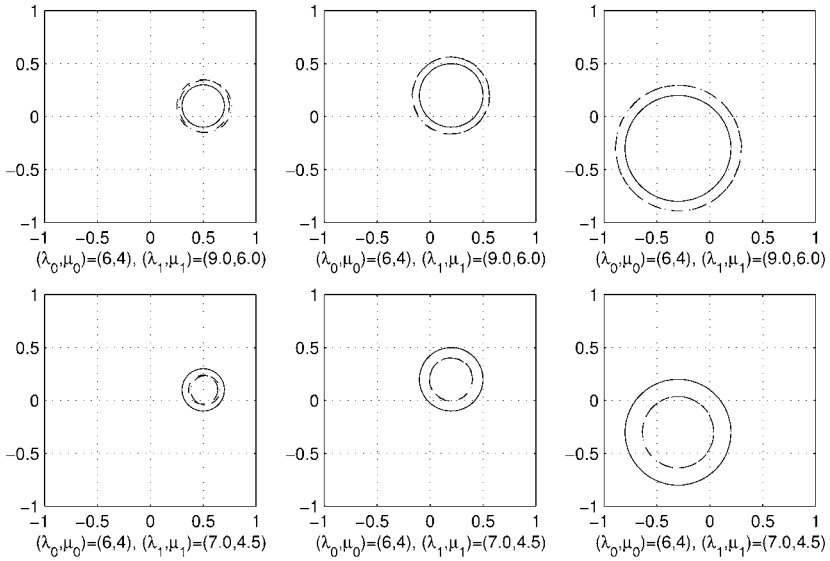

Figure 4. Reconstruction results. Dash–dotted circles by the linear method and dashed circles by the quadratic method. The three upper cases have stiff inclusions with $(\tilde{\lambda}, \tilde{\mu}) = (9, 6)$, $(\lambda, \mu) = (6, 4)$ and the three lower cases are with $(\tilde{\lambda}, \tilde{\mu}) = (6, 4)$, $(\lambda, \mu) = (9, 6)$. We use the notation λ_0, μ_0 for λ, μ and λ_1, μ_1 for $\tilde{\lambda}$, $\tilde{\mu}$.

Table 1. Computational results.

(λ, μ)	$(\tilde{\lambda}, \tilde{\mu})$	(x, y)	r	r^c	(x_1^c, y_1^c)	(x_2^c, y_2^c)
(6, 4)	(9.0, 6.0)	(0.5, 0.1)	0.2	0.2474	(0.5198, 0.0967)	(0.4988, 0.1014)
(6, 4)	(9.0, 6.0)	(0.2, 0.2)	0.3	0.3638	(0.1999, 0.1999)	(0.1962, 0.1982)
(6, 4)	(9.0, 6.0)	(−0.3, −0.3)	0.5	0.5931	(−0.2974, −0.2972)	(−0.2947, −0.2981)
(6, 4)	(7.0, 4.5)	(0.5, 0.1)	0.2	0.1371	(0.5203, 0.0967)	(0.4995, 0.1009)
(6, 4)	(7.0, 4.5)	(0.2, 0.2)	0.3	0.2029	(0.2003, 0.2003)	(0.1969, 0.1977)
(6, 4)	(7.0, 4.5)	(−0.3, −0.3)	0.5	0.3366	(−0.3006, −0.3005)	(−0.2990, −0.2995)

and not on λ_1. The dependence of size on μ_1 is not known exactly in (3.14) but numerical computation shows that the proportional constant is similar to $\frac{\mu_0+\mu_1}{\mu_0(\mu_0+\mu_1)}$. Therefore, we can compute the radius of inclusion much more precisely using (3.15) when the Lamé constant of the inclusion is known.

Example 4 (General domain cases). We now test the disc reconstruction algorithm with non-circular shape inclusions even though the algorithm has been derived for circular inclusions. The computational results on the 64×64 grid in figure 7 show fairly good agreement with their circular approximations. It is also worth mentioning that $(\lambda_0, \mu_0) = (6, 4)$, $(\lambda_1, \mu_1) = (9, 6)$ gives about 20% bigger results and $(\lambda_0, \mu_0) = (4, 6)$, $(\lambda_1, \mu_1) = (6, 9)$ about 50% bigger than originally, in the disc cases shown in figure 5, therefore the computed results are bigger than the inclusions, especially for the three lower examples.

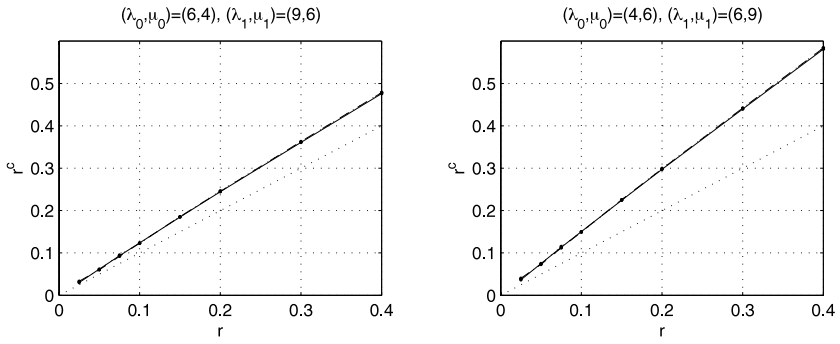

Figure 5. Computed radius r^c on three different computational grids. The dotted line for 48×48, dashed line for 64×64, and solid line for the 128×128 grid coincide well.

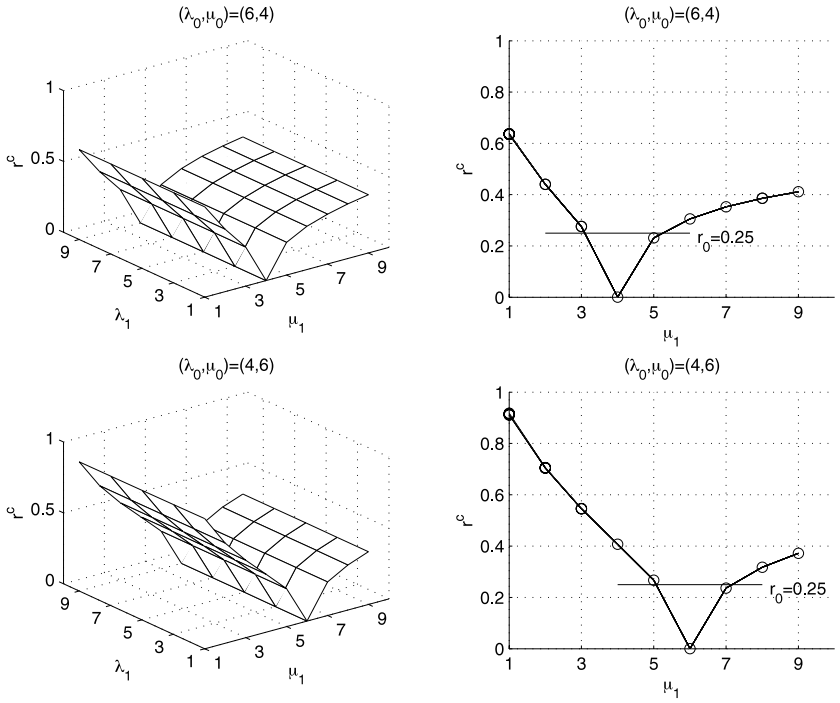

Figure 6. Computed radius as a function of λ_1 and μ_1 for the inclusion of radius $r = 0.25$ centred at $(0.4, 0.2)$. The right-hand plots are the same as their left-hand counterparts, but from different viewpoints.

5. Reconstruction by ellipses

In the previous section, we showed that m_{pq}^{ij} and the centre and size of an inclusion can be detected by the boundary measurements. However, EMTs carry more information of the domain than just the size. For example, if D is an ellipse, then the EMT varies depending on the ratio of the long and short axes. In this section, we propose a method to find an ellipse which represents the detected EMT. For that purpose we first compute the EMTs associated with ellipses. We note that the EMTs associated with elliptic holes with $\tilde{\lambda} = \tilde{\mu} = 0$ were computed in [8] and [10].

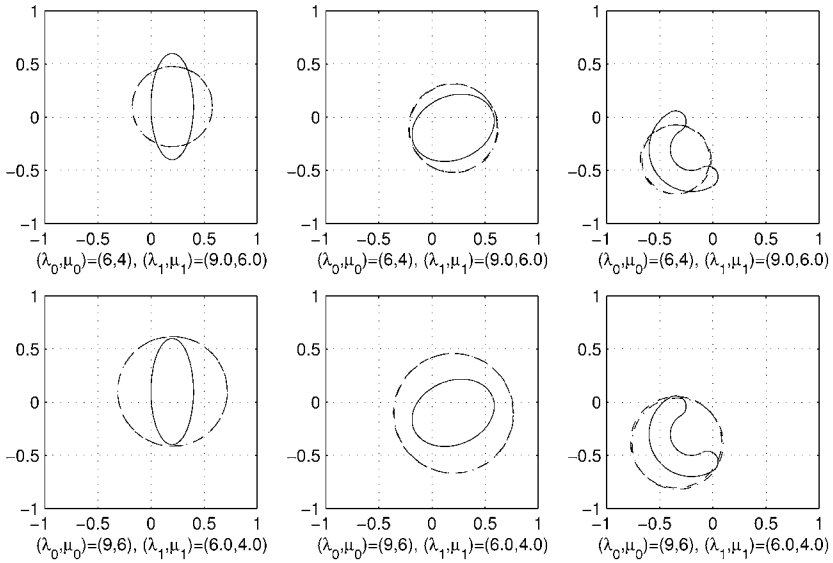

Figure 7. Reconstruction of general shape inclusion.

Let us now restrict ourselves to the two-dimensional case. Suppose that Ω is a domain (bounded or unbounded) with the Lamé parameters λ, μ and let $\vec{u} = (u, v)$ be a solution of $\mathcal{L}_{\lambda,\mu}\vec{u} = 0$ in Ω. By section 32 of [12], there are holomorphic functions φ and ψ in Ω such that

$$2\mu(u + \mathrm{i}v)(z) = \kappa\varphi(z) - z\overline{\varphi'(z)} - \overline{\psi(z)}, \qquad \kappa = \frac{\lambda + 3\mu}{\lambda + \mu}, z = x + \mathrm{i}y. \tag{5.1}$$

Let $\hat{D}$ be the ellipse given by

$$\hat{D} : \frac{x^2}{a^2} + \frac{y^2}{b^2} = 1, \qquad a, b > 0. \tag{5.2}$$

We denote by $\hat{m}^{ij}_{pq}$, $i, j, p, q = 1, 2$, the EMTs associated with $\hat{D}$. Let $\vec{u} = (u, v)$ be the solution of (2.15). Let $\vec{u}_e := \vec{u}|_{\mathbb{C}\setminus\hat{D}}$ and $\vec{u}_i := \vec{u}|_{\hat{D}}$. Then there are functions φ_e and ψ_e holomorphic in $\mathbb{C}\setminus\bar{\hat{D}}$ and φ_i and ψ_i holomorphic in $\hat{D}$ such that

$$2\mu(u_e + \mathrm{i}v_e)(z) = \kappa\varphi_e(z) - z\overline{\varphi_e'(z)} - \overline{\psi_e(z)}, \qquad \kappa = \frac{\lambda + 3\mu}{\lambda + \mu}, z \in \mathbb{C}\setminus\bar{\hat{D}} \tag{5.3}$$

$$2\tilde{\mu}(u_i + \mathrm{i}v_i)(z) = \tilde{\kappa}\varphi_i(z) - z\overline{\varphi_i'(z)} - \overline{\psi_i(z)}, \qquad \kappa = \frac{\tilde{\lambda} + 3\tilde{\mu}}{\tilde{\lambda} + \tilde{\mu}}, z \in \hat{D}. \tag{5.4}$$

It then follows from the transmission condition in (2.15) that the following identity holds on $\partial\hat{D}$:

$$\frac{1}{2\mu}(\kappa\varphi_e(z) - z\overline{\varphi_e'(z)} - \overline{\psi_e(z)}) = \frac{1}{2\tilde{\mu}}(\tilde{\kappa}\varphi_i(z) - z\overline{\varphi_i'(z)} - \overline{\psi_i(z)}). \tag{5.5}$$

Another transmission condition, namely, the continuity of the conormal derivatives along ∂D, takes the form

$$\varphi_e(z) + z\overline{\varphi_e'(z)} + \overline{\psi_e(z)} = \varphi_i(z) + z\overline{\varphi_i'(z)} + \overline{\psi_i(z)} + \mathrm{i}c, \tag{5.6}$$

where c is a constant (see section 32 of [12]).

In order to find the φ_e, ψ_e, φ_i and ψ_i satisfying (5.5) and (5.6), we use elliptic coordinates as used in [12]. Using the notation in [12], let

$$R := \frac{1}{2}(a+b), \qquad m := \frac{a-b}{a+b}, \tag{5.7}$$

and define

$$z = x + \mathrm{i}y = \omega(\zeta) := R\left(\zeta + \frac{m}{\zeta}\right).$$

Then ω maps the exterior of the unit disc onto $\mathbb{C}\backslash\bar{\hat{D}}$.

Lemma 5.1. *For a given pair of complex numbers α and β, there are unique complex numbers A, B, C, E, F such that functions φ_e, ψ_e, φ_i and ψ_i defined by*

$$\varphi_e \circ \omega(\zeta) = R\left[\alpha\zeta + \frac{A}{\zeta}\right], \qquad |\zeta| > 1, \tag{5.8}$$

$$\psi_e \circ \omega(\zeta) = R\left[\beta\zeta + \frac{B}{\zeta} + \frac{C\zeta}{\zeta^2 - m}\right], \qquad |\zeta| > 1, \tag{5.9}$$

$$\varphi_i(z) = Ez, \qquad z \in \hat{D}, \tag{5.10}$$

$$\psi_i(z) = Fz, \qquad z \in \hat{D} \tag{5.11}$$

satisfy the conditions (5.5) and (5.6). Here c in (5.6) can be taken to be zero.

Remark. The numbers α and β determine the intensity and the angle of remote stress (see section 36 of [12]).

Proof of lemma 5.1. Since

$$\frac{\omega(\zeta)}{\overline{\omega'(\zeta)}} = \frac{\zeta^2 + m}{\zeta(1 - m\zeta^2)}, \qquad |\zeta| = 1,$$

the transmission conditions (5.5) and (5.6) are equivalent to the following algebraic equations:

$$\begin{aligned}
&\frac{\kappa}{2\mu}\alpha - \frac{1}{2\mu}\left(\frac{\bar{A}}{m} + \bar{B}\right) = \frac{\tilde{\kappa}E - \bar{E}}{2\tilde{\mu}} - \frac{m}{2\tilde{\mu}}\bar{F},\\
&\alpha + \left(\frac{\bar{A}}{m} + \bar{B}\right) = E + \bar{E} + m\bar{F},\\
&\frac{\kappa}{2\mu}A - \frac{1}{2\mu}(m\bar{\alpha} + \bar{\beta}) = m\frac{\tilde{\kappa}E - \bar{E}}{2\tilde{\mu}} - \frac{1}{2\tilde{\mu}}\bar{F},\\
&A + (m\bar{\alpha} + \bar{\beta}) = m(E + \bar{E}) + \bar{F},\\
&(m^2 + 1)\alpha - \left(m + \frac{1}{m}\right)A + C = 0.
\end{aligned} \tag{5.12}$$

It is easy to show that this system of algebraic equations has a unique solution. The proof is complete. □

Let $\alpha = \alpha_1 + \mathrm{i}\alpha_2$, and so on. Observe that the exterior solution $u_e + \mathrm{i}v_e$ behaves at infinity as

$$\begin{aligned}
u_e(z) + \mathrm{i}v_e(z) = {}& \frac{1}{2\mu}[(\kappa\alpha_1 - \alpha_1 - \beta_1)x + (-\kappa\alpha_2 - \alpha_2 + \beta_2)y]\\
&+ \frac{\mathrm{i}}{2\mu}[(\kappa\alpha_2 + \alpha_2 + \beta_2)x + (\kappa\alpha_1 - \alpha_1 + \beta_1)y] + \mathrm{O}(|z|^{-1}).
\end{aligned} \tag{5.13}$$

We also observe that the interior solution $u_i + \mathrm{i}v_i$ is given by

$$u_i(z) + \mathrm{i}v_i(z) = \frac{1}{2\tilde{\mu}}[((\tilde{\kappa}-1)E_1 - F_1)x + (F_2 - (\tilde{\kappa}+1)E_2)y] + \frac{\mathrm{i}}{2\tilde{\mu}}[((\tilde{\kappa}+1)E_2 + F_2)x + ((\tilde{\kappa}-1)E_1 + F_1)y]. \tag{5.14}$$

Define

$$m_{pq}(\alpha, \beta) := \int_{\partial\hat{D}} \left[\frac{\partial(x_p e_q)}{\partial \nu} - \frac{\partial(x_p e_q)}{\partial \tilde{\nu}}\right] \cdot (u_e, v_e)\, \mathrm{d}\sigma. \tag{5.15}$$

Let $\hat{m}^{ij}_{pq}$ be the EMT associated with $\hat{D}$. Then by (2.16) and (5.13), we have

$$\hat{m}^{11}_{pq} = m_{pq}\left(\frac{\mu}{\kappa-1}, -\mu\right), \qquad \hat{m}^{22}_{pq} = m_{pq}\left(\frac{\mu}{\kappa-1}, \mu\right), \qquad \hat{m}^{12}_{pq} = m_{pq}\left(\frac{-\mathrm{i}\mu}{\kappa-1}, \mathrm{i}\mu\right). \tag{5.16}$$

Since $\vec{u}_e = \vec{u}_i$ on $\partial\hat{D}$, we have

$$\begin{aligned} m_{pq}(\alpha, \beta) &= \int_{\partial\hat{D}} \left[\frac{\partial(x_p e_q)}{\partial \nu} - \frac{\partial(x_p e_q)}{\partial \tilde{\nu}}\right] \cdot \vec{u}_i\, \mathrm{d}\sigma \\ &= \int_{\hat{D}} (\lambda - \tilde{\lambda})\mathrm{div}(x_p e_q)\mathrm{div}(\vec{u}_i) \\ &\quad + \frac{\mu - \tilde{\mu}}{2}(\nabla(x_p e_q) + \nabla(x_p e_q)^{\mathrm{T}}) \cdot (\nabla\vec{u}_i + \nabla\vec{u}_i^{\mathrm{T}})\, \mathrm{d}\sigma. \end{aligned}$$

Denote the solutions of (5.12), which depend on given α and β, by $A = A(\alpha, \beta)$, etc. Then we obtain

$$\frac{\tilde{\mu}}{|\hat{D}|} m_{pq}(\alpha, \beta) = \begin{cases} (\tilde{\kappa}-1)(\lambda - \tilde{\lambda} + \mu - \tilde{\mu})E_1 - (\mu - \tilde{\mu})F_1, & \text{if } p = q = 1, \\ (\mu - \tilde{\mu})F_2, & \text{if } p \neq q, \\ (\tilde{\kappa}-1)(\lambda - \tilde{\lambda} + \mu - \tilde{\mu})E_1 + (\mu - \tilde{\mu})F_1, & \text{if } p = q = 2. \end{cases} \tag{5.17}$$

For given α, β, we solve the system of linear equations (5.12) to find $E(\alpha, \beta)$ and $F(\alpha, \beta)$, and using (5.16) and (5.17) we can find $\hat{m}^{ij}_{pq}$, $i, j, p, q = 1, 2$.

Lemma 5.2. *If $\hat{D}$ is as above, then*

$$\hat{m}^{12}_{11} = \hat{m}^{12}_{22} = 0. \tag{5.18}$$

Moreover, if $\hat{D}$ is a disc, then in addition to (5.18) the following relations hold:

$$\hat{m}^{11}_{11} = \hat{m}^{22}_{22} = \hat{m}^{11}_{22} + 2\hat{m}^{12}_{12}. \tag{5.19}$$

Proof. Since the coefficients of (5.12) are real, $E_1(\alpha, \beta) = F_1(\alpha, \beta) = 0$ if α and β are purely imaginary, and $E_2(\alpha, \beta) = F_2(\alpha, \beta) = 0$ if α and β are real. Thus (5.18) follows from (5.16) and (5.17).

Let $D = R_\theta(\hat{D})$. Then it follows from (2.17) and (5.18) that

$$\begin{aligned} m^{11}_{11} &= \cos^4\theta\hat{m}^{11}_{11} + \tfrac{1}{2}\sin^2(2\theta)\hat{m}^{11}_{22} + \sin^2(2\theta)\hat{m}^{12}_{12} + \sin^4\theta\hat{m}^{22}_{22}, \\ m^{11}_{12} &= \sin\theta\cos^3\theta\hat{m}^{11}_{11} - \tfrac{1}{4}\sin(4\theta)\hat{m}^{11}_{22} - \tfrac{1}{2}\sin(4\theta)\hat{m}^{12}_{12} - \sin^3\theta\cos\theta\hat{m}^{22}_{22}, \\ m^{11}_{22} &= \tfrac{1}{2}\sin^2(2\theta)\hat{m}^{11}_{11} + (1 - \tfrac{1}{2}\sin^2(2\theta))\hat{m}^{11}_{22} - \sin^2(2\theta)\hat{m}^{12}_{12} + \tfrac{1}{2}\sin^2(2\theta)\hat{m}^{22}_{22}, \\ m^{12}_{12} &= \tfrac{1}{2}\sin^2(2\theta)\hat{m}^{11}_{11} - \tfrac{1}{2}\sin^2(2\theta)\hat{m}^{11}_{22} + \cos^2(2\theta)\hat{m}^{12}_{12} + \tfrac{1}{4}\sin^2(2\theta)\hat{m}^{22}_{22}, \\ m^{12}_{22} &= \sin^3\theta\cos\theta\hat{m}^{11}_{11} + \tfrac{1}{4}\sin(4\theta)\hat{m}^{11}_{22} + \tfrac{1}{2}\sin(4\theta)\hat{m}^{12}_{12} - \sin\theta\cos^3\theta\hat{m}^{22}_{22}, \\ m^{22}_{22} &= \sin^4\theta\hat{m}^{11}_{11} + \tfrac{1}{2}\sin^2(2\theta)\hat{m}^{11}_{22} + \sin^2(2\theta)\hat{m}^{12}_{22} + \cos^4\theta\hat{m}^{22}_{22}. \end{aligned} \tag{5.20}$$

If D is a disc, then $m^{ij}_{pq} = \hat{m}^{ij}_{pq}$, $i, j, p, q = 1, 2$, for any θ. Thus one can read (5.19) from (5.20). This completes the proof. □

Lemma 5.3. *Suppose that either $m_{12}^{11} + m_{22}^{12}$ or $m_{11}^{11} - m_{22}^{22}$ is not zero. Then*

$$\frac{m_{12}^{11} + m_{22}^{12}}{m_{11}^{11} - m_{22}^{22}} = \frac{1}{2}\tan 2\theta. \tag{5.21}$$

Proof. One can easily see from (5.20) that

$$m_{11}^{11} - m_{22}^{22} = \cos 2\theta(\hat{m}_{11}^{11} - \hat{m}_{22}^{22}), \qquad m_{12}^{11} + m_{22}^{12} = \tfrac{1}{2}\sin 2\theta(\hat{m}_{11}^{11} - \hat{m}_{22}^{22}).$$

Thus we get (5.21). □

Representing an ellipse

We now describe a method to find an ellipse which represents the detected EMTs. Let M_{pq}^{ij}, $i, j, p, q = 1, 2$, be the detected EMTs. Let $\hat{m}_{pq}^{ij}$ be the EMT associated with the ellipse $\hat{D}$ of the form (5.2), and let m_{pq}^{ij} be the EMT associated with $D := R_\theta(\hat{D})$. Then m_{pq}^{ij} are determined by θ, $|D|$, and m defined by (5.7). For convenience, set $\eta := |D|$.

First we set a tolerance by τ. If both $|M_{12}^{11} + M_{22}^{12}|$ and $|M_{11}^{11} - M_{22}^{22}|$ are smaller than τ, then represent the EMTs by the disc of the size found in the previous section.

If either $|M_{12}^{11} + M_{22}^{12}|$ or $|M_{11}^{11} - M_{22}^{22}|$ is larger than τ, then first find the angle of rotation θ by solving (5.21), namely

$$\frac{M_{12}^{11} + M_{22}^{12}}{M_{11}^{11} - M_{22}^{22}} = \frac{1}{2}\tan 2\theta, \qquad 0 \leqslant \theta < \frac{\pi}{2}. \tag{5.22}$$

We then compute $\hat{M}_{pq}^{ij}$ by reversing the rotation by θ found in (5.22). Since it suffices to replace r_{ij} with $(-1)^{i+j}r_{ij}$ in (2.17), we get

$$\hat{M}_{pq}^{ij} = \sum_{u,v=1}^{2}\sum_{k,l=1}^{2}(-1)^{u+k+p+i} r_{pu} r_{vq} r_{ik} r_{lj} M_{uv}^{kl}, \tag{5.23}$$

where

$$\begin{pmatrix} r_{11} & r_{12} \\ r_{21} & r_{22} \end{pmatrix} = \begin{pmatrix} \cos\theta & -\sin\theta \\ \sin\theta & \cos\theta \end{pmatrix}.$$

The ideal next step would be to use (5.16) and (5.17) to find $\eta = |D|$ and m which produce $\hat{m}_{pq}^{ij}$ which best fit to $\hat{M}_{pq}^{ij}$, or which minimize

$$|\hat{m}_{11}^{11} - \hat{M}_{11}^{11}| + |\hat{m}_{22}^{22} - \hat{M}_{22}^{22}| + |\hat{m}_{22}^{11} - \hat{M}_{22}^{11}| + |\hat{m}_{12}^{12} - \hat{M}_{12}^{12}|. \tag{5.24}$$

But it is not so clear how to minimize (5.24) since $\hat{m}_{pq}^{ij}$ is a nonlinear function of m and η. So we propose a different method to find η and m.

The relation (5.19) suggests that $2(\hat{m}_{22}^{11} + 2\hat{m}_{12}^{12}) - (\hat{m}_{11}^{11} + \hat{m}_{22}^{22})$ carries some information on the size of m, the ratio of long and short axes, while m_{12}^{12} carries information on η, the size of D. So, we solve

$$2(\hat{m}_{22}^{11} + 2\hat{m}_{12}^{12}) - (\hat{m}_{11}^{11} + \hat{m}_{22}^{22}) = 2(\hat{M}_{22}^{11} + 2M_{12}^{12}) - (M_{11}^{11} + \hat{M}_{22}^{22}) \qquad \hat{m}_{12}^{12} = \hat{M}_{12}^{12}. \tag{5.25}$$

Among the solutions found by solving (5.25), we choose the one which minimizes (5.24).

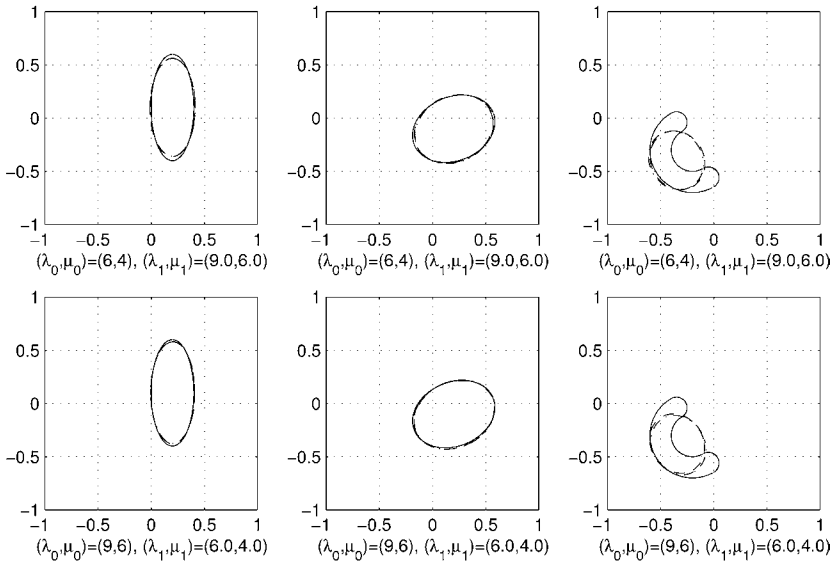

Figure 8. Computed ellipses for various inclusions marked with solid curves. The centres of dotted ellipses are computed by the linear method and dash–dotted ones by the quadratic method

6. Computational examples

The computational algorithm to reconstruct an ellipse has also been implemented using Matlab. The algorithm first computes the centre of an ellipse using linear solutions or a quadratic solution, which is an identical procedure to the disc reconstruction method, then tries to recover the major and minor axes, and the orientation of the ellipse. Thus we cannot expect any better result for the centre of the ellipse; however, the shape and orientation of the ellipse can be recovered more precisely than with the disc reconstruction algorithm.

Example 5 (Ellipse reconstruction). In this example, we test the algorithm using the same domains as in example 4. The ellipse reconstruction method can be summarized as follows.

Let M_{pq}^{ij} be the detected EMT. Given a tolerance τ, if both $|M_{12}^{11}+M_{22}^{12}|$ and $|M_{11}^{11}-M_{22}^{22}|$ are smaller than τ, then find the disc of the size found in the previous section. If either $|M_{12}^{11}+M_{22}^{12}|$ or $|M_{11}^{11}-M_{22}^{22}|$ is larger than τ, then

(E1) Determine the angle of rotation θ by solving (5.22),

$$\frac{M_{12}^{11}+M_{22}^{12}}{M_{11}^{11}-M_{22}^{22}}=\frac{1}{2}\tan 2\theta, \qquad 0\leqslant\theta<\frac{\pi}{2}.$$

(E2) Using the angle θ found in (E1), solve (5.23) to find $\hat{M}_{pq}^{ij}$:

$$\hat{M}_{pq}^{ij}=\sum_{u,v=1}^{2}\sum_{k,l=1}^{2}(-1)^{u+k+p+i}r_{pu}r_{vq}r_{ik}r_{lj}M_{uv}^{kl},$$

where

$$\begin{pmatrix} r_{11} & r_{12} \\ r_{21} & r_{22} \end{pmatrix}=\begin{pmatrix} \cos\theta & -\sin\theta \\ \sin\theta & \cos\theta \end{pmatrix}.$$

(E3) Find $|D|$ and m by solving (5.25):

$$2(\hat{m}_{22}^{11} + 2\hat{m}_{12}^{12}) - (\hat{m}_{11}^{11} + \hat{m}_{22}^{22}) = 2(\hat{M}_{22}^{11} + 2M_{12}^{12}) - (M_{11}^{11} + \hat{M}_{22}^{22}) \qquad \hat{m}_{12}^{12} = \hat{M}_{12}^{12}.$$

(E4) Among the solutions in (E3), choose the one minimizing (5.24),

$$|\hat{m}_{11}^{11} - \hat{M}_{11}^{11}| + |\hat{m}_{22}^{22} - \hat{M}_{22}^{22}| + |\hat{m}_{22}^{11} - \hat{M}_{22}^{11}| + |\hat{m}_{12}^{12} - \hat{M}_{12}^{12}|.$$

Figure 8 shows the reconstructed ellipses. The algorithm gives perfect reconstruction results for elliptic inclusions and fairly good approximation even for non-elliptic domains in the sense that it provides correct estimations on the major and minor axes, and the orientation. It is worth remarking that the ellipse reconstruction method requires Lamé constants not only for the background but also of the inclusion while the disc reconstruction method uses only background information. Thus, it is not surprising that this ellipse method gives perfect size information for the discs, as shown in the first diagram in figure 8.

7. Conclusion

In this paper we consider the problem of identifying unknown inclusions inside an elastic body. An inclusion has different Lamé parameters from those of the background. Based on the asymptotic formula in [3], we propose an algorithm to detect the EMT and the location of the inclusion. The algorithm proposed in this paper uses quadratic polynomials to detect the location while that in [3] only uses linear tractions. We implemented both algorithms and compared the results.

In order to estimate the size of the inclusion, we use m_{12}^{12} based on an estimate in [3]. For the same purpose we may use the average of the trace, namely $\frac{1}{4}(m_{11}^{11} + 2m_{12}^{12} + m_{22}^{22})$. Since mere size estimation does not represent the estimated EMTs fully, we propose another algorithm to identify an ellipse which can represent them. It turns out that the algorithm identifies the ellipse rather well by representing the orientation, and long and short axes of the inclusion. We should mention that in the case of conductors there is a one-to-one correspondence between the class of ellipses and the two-dimensional polarization tensors, see [6] and [11]. By finding two eigenvalues and two linearly independent eigenvectors, we can identify the ellipse corresponding to the detected polarization tensor. But for two-dimensional EMTs, there are three nonzero eigenvalues and three corresponding eigenvectors. It would be interesting to find a class of geometric figures which can be uniquely identified by these eigenvectors and eigenfunctions.

Acknowledgments

HK was partly supported by KOSEF 98-0701-03-5 and JYL by KOSEF R11-2002-103.

References

[1] Alves C and Ammari H 2002 Boundary integral formulae for the reconstruction of imperfections of small diameter in an elastic medium *SIAM J. Appl. Math.* **62** 94–106

[2] Ammari H, Kang H and Nakamura G, in preparation

[3] Ammari H, Kang H, Nakamura G and Tanuma K 2003 Complete asymptotic expansions of solutions of the system of elastostatics in the presence of an inclusion of small diameter and detection of an inclusion *J. Elast.* at press

[4] Ammari H, Moskow S and Vogelius M 2003 Boundary integral formulas for the reconstruction of electromagnetic imperfections of small diameter *ESAIM: Cont. Opt. Calc. Var.* **9** 49–66

[5] Ammari H and Seo J K 2003 A new formula for the reconstruction of conductivity inhomogeneities *Adv. Appl. Math.* at press

[6] Brühl M, Hanke M and Vogelius M S 2003 A direct impedance tomography algorithm for locating small inhomogeneities *Numer. Math.* **93** 635–54

[7] Kwon O, Seo J K and Yoon J R 2002 A real-time algorithm for the location search of discontinuous conductivities with one measurement *Commun. Pure Appl. Math.* **55** 1–29
[8] Lewiński T and Sokolowski J 2002 Energy change due to the appearance of cavities in elastic solids *Preprint*
[9] Maz'ya V G and Nazarow S A 1988 The asymptotic behaviour of energy integrals under small perturbations of the boundary near corner points and conical points *Tr. Moskovsk. Matem. Obshch.* **50** (in Russian) (Engl. transl. 1988 *Trans. Moscow Math. Soc.* 77–127)
[10] Movchan A B and Movchan N V 1995 *Mathematical Modelling of Solids with Nonregular Boundaries* (Boca Raton, FL: Chemical Rubber Company Press)
[11] Movchan A B and Serkov S K 1997 The Pólya–Szegö matrices in asymptotic models of dilute composite *Euro. J. Appl. Math.* **8** 595–621
[12] Muskhelishvili N I 1977 *Some Basic Problems of the Mathematical Theory of Elasticity* (Leyden: Noordhoff) (Engl. transl.)